


Article

Modification of Hardwood Derived Biochar to Improve Phosphorus Adsorption

Laura Arbelaez Breton ¹, Zainab Mahdi ¹, Chris Pratt ^{2,3} and Ali El Hanandeh ^{1,*} 

¹ School of Engineering and Built Environment, Griffith University, Nathan, QLD 4111, Australia; lauambiental@gmail.com (L.A.B.); z.mahdi@griffith.edu.au (Z.M.)

² School of Environment and Science, Griffith University, Nathan, QLD 4111, Australia; c.pratt@griffith.edu.au

³ Australian Rivers Institute, Griffith University, Nathan, QLD 4111, Australia

* Correspondence: a.elhanandeh@griffith.edu.au

Abstract: The excessive application of phosphorus in agricultural lands leads to serious environmental issues. Efficient application is beneficial from an economic and environmental perspectives. Biochar can be used as a carrier for slow release of phosphate. However, its adsorption capacity is limited. In this work, biochar was prepared at different pyrolysis temperatures (350–550 °C). The biochar prepared at 550 °C had the highest adsorption capacity and was selected for modification by magnesium impregnation. Magnesium modification enhanced the adsorption capacity by 34% to a theoretical max adsorption capacity of 463.5 mg·g^{−1}. The adsorbed phosphate can be desorbed. The desorption was bi-phasic with fast- and slow-release fractions. The distribution of the phosphate fractions was pH dependent with slow release being most prominent in neutral conditions. Mg modified biochar can be used to recover phosphate and then used as a carrier for slow release of phosphate. The bi-phasic desorption behaviour is useful as the fast release fraction can provide the immediate phosphate needed during plant establishment, while the slow-release fraction maintains steady supply over extended periods.

Keywords: phosphorus recovery; adsorption; biochar; modification; Mg modified biochar



Citation: Arbelaez Breton, L.; Mahdi, Z.; Pratt, C.; El Hanandeh, A. Modification of Hardwood Derived Biochar to Improve Phosphorus Adsorption. *Environments* **2021**, *8*, 41. <https://doi.org/10.3390/environments8050041>

Academic Editors: Nelson Belzile and Wen-tien Tsai

Received: 10 February 2021

Accepted: 2 May 2021

Published: 6 May 2021

Publisher's Note: MDPI stays neutral with regard to jurisdictional claims in published maps and institutional affiliations.



Copyright: © 2021 by the authors. Licensee MDPI, Basel, Switzerland. This article is an open access article distributed under the terms and conditions of the Creative Commons Attribution (CC BY) license (<https://creativecommons.org/licenses/by/4.0/>).

1. Introduction

Phosphate is an essential and irreplaceable nutrient required for plants development and growth. However, it has become a matter of major concern due to the rapid depletion of phosphorus reserves, the increasing demand for fertiliser in the agricultural sector and the negative environmental impacts it has in water bodies (eutrophication) [1–3]. Therefore, in terms of coping with the increasing demand for fertiliser and minimising the environmental impact caused by phosphate runoff, different approaches should be employed to ensure effective delivery of the phosphate as needed.

Biochar is an organic porous material, resulting from the thermochemical conversion or thermal decomposition of biomass in a limited oxygen environment. It is a solid and carbon-rich material which can be used as an adsorbent agent because of its physicochemical properties such as high surface area and cation exchange capacity [4]. Wu and Wei [5] presented several benefits of biochar, among them it helps to improve fertility in soils, contributes to reduce nutrient leaching—a major cause for eutrophication in water bodies—and improves crop production. Other soil and environmental benefits of biochar are shown in Figure 1. Because of all its potential uses and benefits, biochar has received much attention as it is perceived as an environmentally sound and low-cost material with promising applications in agricultural and environmental fields [4,6,7]. When placed in the soil, biochar can hold carbon for thousands of years as well as retaining nutrients for the plant; this makes it more stable and effective than other organic matters used as fertilisers, such as compost and manure [8]. In addition, biochar has also been shown to enhance soil physical properties such as porosity, water holding capacity and soil aggregate

stability [9,10]. Therefore, biochar has potential as a soil amendment contributing to long term soil fertility for plants under drought conditions. However, most studies are focused on enhancing biochar phosphate adsorption and less attention has been given to phosphate desorption processes [2,11]. Understanding not only the adsorption of phosphate by biochar but also how this recovered phosphate can be effectively released (desorption) will improve phosphate management in soils as well as its bioavailability for plants and crops in the future.

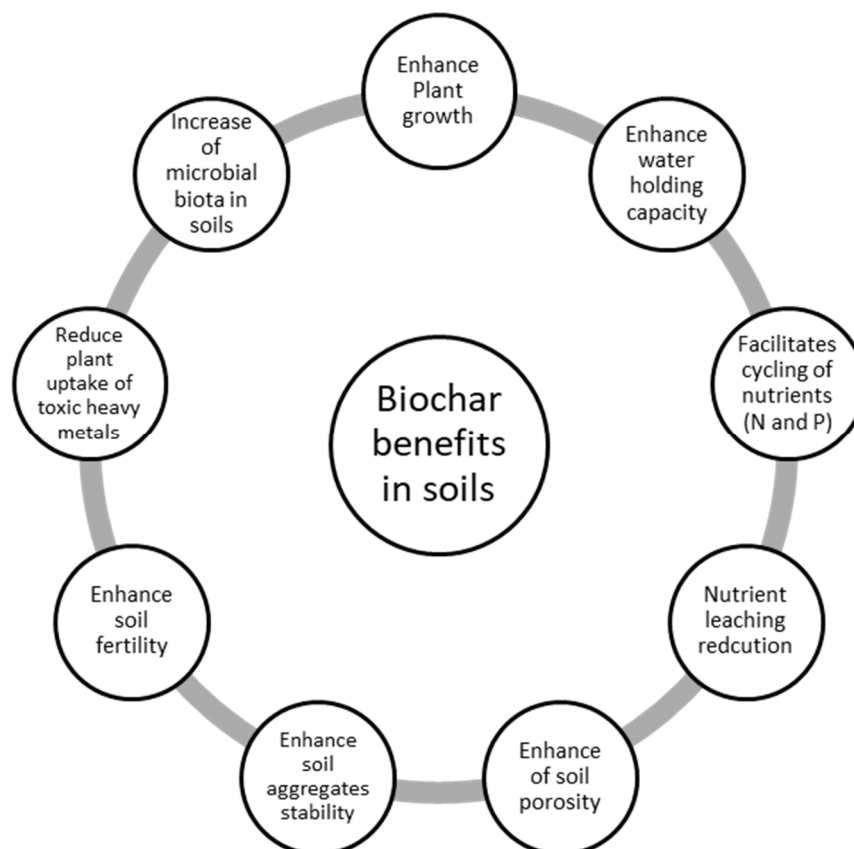


Figure 1. Potential biochar benefits in soils. Adapted from [9,10,12].

For the synthesis of modified biochar, different kinds of biomass have been used, among these are sludge waste, agricultural waste (e.g., wheat, corn and sugar beet tailing), animal litter and wood waste. Wood waste has been used in different studies to harness its capacity for phosphate adsorption as well as its properties as biochar [12]. This material has various advantages for the production of biochar as it contains low moisture and ash content and has shown promising results for the adsorption of phosphate with adsorption concentrations of 118 and 142.7 mg-P·g⁻¹ by woody biochar derived from oak sawdust and wood waste, respectively [13,14].

Woody residue can be found in the form of sawdust, woodchip, shavings and bark. Apart from its low cost and high availability, hardwood has presented promising results when used for the synthesis of biochar for the adsorption of phosphate. Dugdug and Chang [15] concluded hardwood biochar had better performance in the adsorption of phosphate compared wheat straw biochar. Therefore, hardwood can be a potential candidate for low-cost biomass to produce modified biochar with the objective of phosphate delivery to crops. This can contribute to addressing the issue of a suitable end-use for this raw material, while acting as a potential source of phosphate for crops located in places under drought stress conditions.

1.1. Biomass Used to Produce Biochar for the Adsorption of Phosphate

Biochar properties and its potential use as a soil amendment for the increase of nutrient availability depends significantly on the type of biomass employed for its synthesis as well as the pyrolysis conditions [15]. Biomass has significant effects on different properties of biochar, including ash content, H/C ratio, pH, surface area and cation and anion exchange capacity according to the authors of [16].

The selection of biomass is paramount to enhance the properties of biochar; the authors of [14] suggested biomass with low moisture content is suitable for biochar synthesis, as it requires low demand of heat energy and time for the pyrolysis, avoiding inhibition of char formation making it a low-cost process. Ash content can also be a determining factor for selecting a biomass source to produce biochar; the authors of [16] studied 12 different biochars produced from different feedstocks and concluded that biochar produced from feedstock with lower ash content can be easily applied in soils as there is less loss by wind. The study recommended woody-based biomass as it showed lower ash content than the non-woody biomass (turkey litter and walnut shell). Similar results are presented in [1], where oak wood biomass had lower ash content compared to greenhouse waste. Furthermore, woody biomass has been reported to produce biochars with higher surface area than other sources such as straw biochar, green waste biochar and algae biochar [16]. Biochar yield is also influenced by the type of feedstock employed. According to the authors of [12], higher yield production of biochar results from the pyrolysis of animal litter and solid wastes biomass than from crop and wood biomass. This can be related to the high inorganic content of waste-based biomass. Table 1 presents a summary of some of the promising material for biochar production for phosphate adsorption.

Table 1. Sources of biomass used for the synthesis of biochar for the adsorption of phosphate, pyrolysis temperature and time.

Biomass	Phosphate Adsorption Capacity $\text{mg-P}\cdot\text{g}^{-1}$	Pyrolysis Temperature $^{\circ}\text{C}$	Pyrolysis Time	References
		Agricultural waste		
Soybean straw	74.47	500	2 h	[6]
Tobacco stems	90.91	750	4 h	[17]
		Animal waste		
Cow dung	240.83	700	1 h	[18]
		Sludge waste		
Waste activated sludge	111	550	2 h	[19]
		Woody		
Oak sawdust	142.7	500	30 min	[20]
Wood chips	3.201	500	2 h	[21]
Wood waste: Populus X Canadensis Moench and Sophora japonica Linn	118	600	1 h	[4]
Oak chips	46.37	500	30 min	[22]

1.2. Adsorption of Phosphate by Biochar

Efficient adsorption of phosphate by raw biochar is low due to its negatively charged surface, lack of compatible functional groups and imperfect porosity structure [5]. Therefore, it is necessary to chemically modify biochar to enhance its phosphate adsorption capacity. A variety of agents have been used to modify biochar to promote phosphate capture, as shown in Table 2, but the use of metals has been the most frequently employed technique because they present high efficiency, low cost and are abundant in the biosphere [23].

The use of magnesium (Mg) has resulted in positive effects on the adsorption of phosphate by biochar. Mg is an abundant, environmentally friendly and low-cost material, with high affinity to phosphate [17]. Wu and Wei [5] reported that modified biochar with

MgO adsorbed twice the rate of raw biochar. Xu and Zhang [4] compared the efficiency of different modification agents (Mg, Al, Fe and Ca) showing Mg-biochar had the best phosphate adsorption capacity. Lanthanum (La), which is a relatively low-cost material, with low harm to the environment and is generally abundant, has also been used to modify biochar for phosphate adsorption. Wang and Guo [20] reported that La modified biochar has 4.5-fold improvement over raw biochar. Other agents used to modify the biochar to enhance its phosphate adsorption capacity include iron (Fe) and aluminium (Al). Table 2 presents some of the latest development in metal-biochar works for phosphate adsorption.

Table 2. P adsorption capacity of biochar using different modification agents.

Biochar Feedstock	Modification/Activation Agents	Phosphate Adsorption Capacity mg-P·g ⁻¹	References
Ground corn biochar	MgCl ₂	239	[24]
Peanut-shells	MgO	18.94	[5]
Poplar chips	MgCl ₂ ·6H ₂ O	89	[25]
Holm oak	MgCl ₂ ·6H ₂ O	64.6	[26]
Greenhouse paprika waste	MgCl ₂ ·6H ₂ O	65.1	[26]
Bamboo feedstock	Mg-Fe LDH	7.58	[27]
Bamboo feedstock	Mg-Al LDH	13.11	[27]
Sesame straw	MgO	8.42	[28]
Pineapple peels	La(OH) ₃	101.16	[29]
Sewage sludge	La(NO ₃) ₃	93.91	[30]
Oak chips	La(NO ₃) ₃	46.37	[22]
Phragmites australis	LaCl ₃ /Fe ₃ O ₄	25	[31]
Powdered straw	LaFeO ₃	209.25	[32]
Waste activated sludge	FeSO ₄ ·7H ₂ O and FeCl ₃ ·6H ₂ O	34.2	[19]
Waste activated sludge	FeCl ₃ ·6H ₂ O	111	[19]
Okara	FeCl ₃	4.785	[33]
Sludge-based biochar	FeSO ₄	3.14	[34]
Sludge-based biochar	Fe(NO ₃) ₃	2.34	[34]
Corn cobs	Fe(NO ₃) ₃	1.99	[21]
Garden wood waste	Fe(NO ₃) ₃	2.75	[21]
Wood chips	Fe(NO ₃) ₃	3.2	[21]
Cotton stalk	FeCl ₃	0.399	[35]
Poultry manure	AlCl ₃	701.65	[36]
Industrial tea waste	Al(NO ₃) ₃ ·9H ₂ O	5	[37]
Sludge-based biochar	Al(NO ₃) ₃	2.69	[34]

1.3. Desorption of Phosphate by Biochar

The desorption process of phosphate by modified biochar is important to understand its potential use as a fertiliser and soil amendment. Different factors can affect the desorption process of nutrients from biochar such as pyrolysis temperature, type of biomass employed and biochar application rate [9]. However, in the literature, studies regarding desorption of phosphate by modified biochar are limited. The information focuses on biochar's recyclability and reusability for the adsorption of phosphate, the cost-efficiency of the adsorption process and the benefits of biochar application for crop development and soil function [3]. Few studies focused on the release of phosphate from biochar for its potential use as a slow-release fertiliser. Hale and Alling [38] reported cacao shell biochar had a phosphate desorption value of 1.48 mg·g⁻¹ and corn cob 0.172 mg·g⁻¹ in two months. Fang et al. [39] reported that the release rate of phosphate by Mg biochar at different pyrolysis temperatures 300, 450 and 600 °C were 3.3% (8 mg·g⁻¹), 3.9% (9.2 mg·g⁻¹) and 4.4% (10.8 mg·g⁻¹), respectively, over a period of 90 h. However, it is important to note that the latter experiments were carried at acidic conditions.

Other studies related to desorption of phosphate have not reported the rate of phosphate release from biochar. Morales and Comerford [11] developed a study of adsorption and desorption of phosphate focused on comparing three different feedstock at different

pyrolysis temperatures. However, desorption analysis was more concentrated on how the biochar characteristics influenced phosphate release rates. Takaya and Fletcher [1] also analysed the desorption process of modified biochar. However, they reported further investigation is required to know its potential uses as a soil fertiliser. Chen and Qin [18] studied the potential of engineered biochar from agricultural waste (cow dung) for the slow release of phosphate and its use as a fertiliser. Biochar produced from cow dung when used as fertiliser in lettuce crops improved phosphate availability, soil pH, soil moisture content and organic carbon content, as well as crop growth and yield.

Despite the promising results, no studies have been conducted to evaluate the desorption rate of modified biochar employing post-treatment by modification agents to enhance its capacity as a potential slow nutrient carrier. Hence, the objective of this project was to synthesise a biochar for the effective adsorption and release of phosphate. In this paper, we report on adsorption and desorption behaviour for a Mg-treated biochar. We envisage that our work will help improve understanding of phosphate availability in agronomic settings, which is highly relevant as alternative and resilient phosphorus fertilisers are sought.

2. Materials and Methods

2.1. Biochar Preparation and MgCl₂ Modified Biochar Preparation

Eucalypt stem tree chips were obtained locally, to produce HW-biochar and HW-modified biochar. This raw material was washed with deionised water (DW) to remove impurities and then oven dried at 105 °C for approximately 24 h. Measured quantities of the biomass was pyrolysed at three different temperatures 350, 450 and 550 °C in a tube furnace in an oxygen starved environment. Pyrolysis was carried out for 1.5 h at 10 °C/min, and then the furnace was allowed to cool to room temperature to retrieve the samples. The yield is calculated as follows:

$$Yield_{Biochar} = \frac{m_{biochar}}{m_{raw\ biomass}} \times 100\%. \quad (1)$$

where $Yield_{Biochar}$ is the mass yield of biochar in per cent, $m_{biochar}$ is mass of biochar in g and $m_{raw\ biomass}$ is the mass of raw biomass in g.

The biochar samples were crushed and sieved into small pieces of 0.5–0.2 mm size. Biochar samples were then submerged in 0.5 M HCl at a ratio of 1 g:10 mL for 24 h to remove impurities and ash and enhance the porous structure. Then, samples were rinsed with DW to remove impurities and oven dried at 105 °C. The raw biochar samples were stored in labelled airtight plastic containers. The modified biochar was prepared by impregnation following procedure described in [24] with slight modification. Briefly, biochar was soaked in 1 M MgCl₂ solution prepared by dissolving 203.3 g of MgCl₂·6H₂O in 1000 mL of DW. The raw biochar sample was submerged into the MgCl₂ [4], with constant shaking for 24 h. Then, the samples were filtered with 90 mm Whatman filter paper, and modified biochar was oven dried at 105 °C for 24 h and stored in containers labelled as Mg-Biochar.

2.2. Biochar Characterisation and Proximate Analysis

The pH of the samples was determined according to the ASTM Standard Method (D3838-05). First, 0.1 g of each sample were added to 10 mL of DW followed by shaking. Then, pH was measured using a pH meter. Fourier-transform infrared spectroscopy (FTIR) was employed for the characterisation of the functional groups of the biochar samples.

Ash content (ASH) of biochar was measured following the ASTM Standard method (D3174) by calculating the difference between the masses after combustion of 1 g of the sample in the furnace at 650 °C for 3 h. The volatile matter (VM) was determined following the ASTM Standard method (D1762-84) by calculating the mass difference after the combustion of 1 g of sample in the furnace at 350 °C for 3 min. Fixed carbon content was calculated as the difference of the total original weigh of the sample and the sum of ASH and VM. Scanning electron microscope (SEM) imaging were used to inspect the surface and structure of the biochar.

2.3. Specific Surface Area and Electron Microscopy

The BET specific surface area (SSA) and pore volume of raw biochar and Mg-biochar was determined using N₂ adsorption at 77 K (Micrometrics TriStar II 3020 3.02, Norcross, GA, USA). Electron microscopy images and scans were obtained using a JEOL JSM7100F scanning electron microscope

2.4. Point of Zero Charge (pH_{PZC})

The Point of zero charge of raw biochar and modified biochar was measured according to procedure described in [39]. First, 0.15 g of each biochar were mixed with 15 mL of 0.01 M NaCl solution with pH range from 2 to 12. The pH was adjusted using 0.1 M of HCl and NaOH. The final pH of the solution was measured after 24 h of shaking.

2.5. Phosphate Adsorption Screening Experiments

Phosphate solution was prepared by dissolving 176.16 g potassium phosphate dibasic anhydrous (K₂HPO₄) in 1 L of DW for the adsorption experiments. Working solutions were prepared from the stock solution as needed. Screening tests were performed to determine the biochar with the highest potential for further investigation; 0.2 g of the samples were loaded into a flask with 20 mL of the phosphorus solution with a concentration of 30 mg·L⁻¹. Then, the containers were put in a shaker and mixed vigorously at room temperature for 24 h. The phosphate adsorption performance was calculated by the difference in concentration between the initial concentration of phosphate and the final concentration. The amount of P adsorbed by the biochar samples (q_e) was calculated using Equation (2):

$$q_e = V(C_0 - C_e) / M \quad (2)$$

where q_e (mg·g⁻¹) is the amount of P adsorbed on biochar, C_0 (mg·L⁻¹) is the initial concentration of P in the solution at starting time ($t = 0$), C_e (mg·L⁻¹) is the final concentration, V (L) is the volume of the P solution and M (g) is the mass of biochar added.

Phosphate concentration was measured following APHA 2005 standard methods. Internal standards were used to validate the results (concentration 0 to 1 mg PO₄-P·L⁻¹). To determine PO₄-P, samples were withdrawn using 0.45 µm filter syringe. The filtered solutions were then analysed using colorimetric methods with a Discrete Chemistry Analyser (Westco Smartchem 200, Danbury, CT, USA). All PO₄³⁻ values are reported as mg-PO₄-P.

2.6. Adsorption Kinetics

P adsorption kinetics was studied following the procedure of Li et al. [26], in which 0.2 g of the biochar sample were added to a solution of 20 mL of a 30 mg PO₄-P·L⁻¹ phosphate solution in a 100 mL flask and then shaken at room temperature. The samples were drawn at 5, 10, 20, 30, 60, 120 and 240 min and 24 h. The kinetics of the adsorption of P were modelled using the pseudo-first- and pseudo-second-order equations (Equations (3) and (4)).

Pseudo-first-order equation:

$$q_t = q_e(1 - e^{-kt}) \quad (3)$$

Pseudo-second-order equation:

$$q_t = \frac{K_2 q_e^2 t}{1 + K_2 q_e t} \quad (4)$$

where q_t is the adsorption capacity at time t (mg·g⁻¹). k and K_2 are the rate constant of pseudo-first order and pseudo-second order, respectively. t is the time (min).

2.7. Adsorption Isotherms

Following the procedure in [25] with modifications, 0.2 g of the adsorbent were added to 20 mL of PO₄-P solution at different concentrations (5, 10, 15, 30 and 50 mg PO₄-P·L⁻¹)

as well as 30 g PO₄-P·L⁻¹. The pH was adjusted by adding 0.1 M of NaOH or HCl as required to maintain pH ~ 6. The samples were drawn, and the total P concentration was measured as described previously. The results were fitted to the Langmuir and Freundlich isotherms models (Equations (5) and (6), respectively):

Langmuir equation:

$$q_e = \frac{q_{max}K_L C_{eq}}{1 + K_L C_{eq}} \quad (5)$$

where q_{max} (mg·g⁻¹) is the monolayer adsorption capacity, C_{eq} (mg·L⁻¹) is the equilibrium concentration of the adsorbate (mg·g⁻¹) and K_L (L·mg⁻¹) is the Langmuir constant.

Freundlich equation:

$$q_e = K_F C_{eq}^{\frac{1}{n}} \quad (6)$$

where K_F is the distribution coefficient (Freundlich adsorption constant) and n is the correction factor.

2.8. Phosphate Desorption Experiments

The desorption experiments were conducted to study the slow-release capacity of biochar. Biochar was first loaded with phosphate by soaking biochar samples in phosphate solutions (20 and 40 mg·L⁻¹) for 24 h at pH = 6. The loaded biochar was first rinsed with DI water and then dried in the oven for 2 h at 105 °C. The amount of phosphate adsorbed onto the biochar were determined by measuring the concentration remaining in the solution. Then, 0.2 g of biochar samples were added to 20 mL DI water and left for different periods of time (5, 30, 60, 180, 360 and 1440 min) at two different pH values (7 and 4.6) to simulate the potential release of phosphate in neutral and acidic environments. The final concentration was measured. The amount of phosphate released can be calculated as $m = C \times V$, where C is the concentration and V is the volume.

2.9. Desorption Kinetics Modelling

To model the kinetics of phosphate desorption, the first rate of decay (FRD) and the two-compartment first-order rate constant (TFRC) models were used. The FRD model is a commonly used decay model which assumes constant rate of release (k) of the adsorbate from the adsorbent over time. The FRD model is mathematically presented as:

$$q_t = q_0 e^{-kt} \quad (7)$$

TFRC is one of the most common empirical equations to obtain the desorption rates [40]. The model assumes bi-phasic release of adsorbate and is represented in the following equation:

$$\frac{q_t}{q_0} = a e^{-k_f t} + (1 - a) e^{-k_s t} \quad (8)$$

q_t is the adsorbate mass per mass adsorbent remaining in the solid phase (mg·g⁻¹) at time t ; q_0 is the initial adsorbate mass held by the adsorbent (mg·g⁻¹); a is the fraction of the fast-desorbing adsorbate; k_f is the first-order desorption rate constant of the fast-desorbing adsorbate (min⁻¹); and k_s is the first-order decay rate of the slow-release adsorbate (min⁻¹).

2.10. Quality Control and Data Analysis

All experiments were run in duplicate and average values are reported. If the difference between the duplicates was more than 10%, the experiment was repeated. To compare the results and determine the significance of the differences before and after treatment, student t -test was used. Analysis of the variance (One-way ANOVA) was used to compare the performance of the different biochars. Significance level ($\alpha = 0.05$) was used in all statistical tests.

3. Results and Discussion

3.1. Biomass and Biochar Properties

The composition of biomass is presented in Table 3. The moisture content of the biomass was 1.73%. Low moisture content is commonly reported in the literature for wood waste biomass [13,14]. The ash content (31.5%) is similar to results reported by Chen and Chen [41] for hardwood (38.55%). Biochar yield for the three different pyrolysis temperatures 350, 450 and 550 °C are shown in Table 3. Biochar yield had an inverse relation with pyrolysis temperature. This behaviour was expected as wood biomass has a high content of cellulose, lignin and hemicellulose [14,42]. In addition, a decrease in yield as the temperature increased can be attributed to great decomposition of primary biomass or to secondary decomposition of biochar according to Ola and Jekayinfa [43]. The P content in the raw biochar ranged 0.0482–0.345 mg·g^{−1}, as shown in Table 3. Experiments were performed to determine the amount of P released from raw biochar to evaluate its availability. The release of P from biochar was very low, thus it is unlikely to be readily available.

Table 3. Proximate composition of biochar at different temperatures.

Proximate Analysis of Dry Biomass (% Dry Basis)	
Ash content	31.5%
Fixed carbon	21%
Volatile matter	47.1%
Yield (%)	
HW-350	71.94%
HW-450	38.21%
HW-550	35.81%
Amount of P (mg·g ^{−1})	
HW-350	0.0482
HW-450	0.0766
HW-550	0.345

The pH of biochar prepared at 350, 450 and 550 °C was alkaline in nature with values 8.1, 8.2 and 8.4, respectively. The increase in pH values with increase in pyrolysis temperature can be caused by the separation of alkali salts from organic materials, as well as the loss of acidic functional groups and the appearance of basic functional groups [42,44]. Oginni and Yakaboylu [45] reported an increase in pH after pyrolysis of wood biomass from longleaf pine, red oak and hard maple at 500 °C; their pH values were 8.6, 9.0 and 9.8, respectively. The modified biochar, Mg-biochar, had alkaline nature (pH = 8.5). Generally, very little change in the pH was observed after the modification process.

Figure 2 shows the SEM and EDS spectrum of the biochar (before modification) with MgCl₂ and after modification (Mg-Biochar). The SEM scans reveal that the pore size of the Mg-Biochar is larger and more developed. Furthermore, the EDS spectra confirms that the Mg presence is more prominent in the Mg-Biochar than in the unmodified biochar.

The specific surface area of the biochar prepared at 500 °C was 1.49 m²·g^{−1} and the pore volume is 0.000427 m³·g^{−1}. Similar results were reported for brown marine macroalgae and woody derived biochar by Oginni and Yakaboylu [45] and Jung and Ahn [7] with SSAs of 2.39 and 0.26 m²·g^{−1}, respectively. For the Mg-biochar (500 °C) produced here, the SSA was 0.97 m²·g^{−1} and the pore volume was 0.0003 m³·g^{−1}. The development of larger pores with wider diameters in the modified can explain the reduction in the BET SSA. As the pore diameter grew, it consumed the smaller pores surrounding it, resulting in loss of nano-surface area. This is not necessarily bad because, for many of the small pores, despite providing higher surface area, the surface area and the active sites within them may not be accessible. Other studies have reflected the influence of residence time and pore clogging to be the some of the causes that affect SSA. Lu and Zong [46]

reported an increase of SSA in maize straw and rice biochar pyrolysed at 550 °C when residence time was increased from 2 to 5 h. Li and Dong [47] noted how high pyrolysis temperatures can cause the pores to collapse reducing the SSA of biochar. Furthermore, it is important to note that the MB method measures the mesoporous surface area of the biochar, which means MB may not reflect the total surface area available for adsorption which includes the micropores. It was also found that the pH_{pzc} of the biochar increased from 7 (raw) to 8 for the Mg-biochar (550 °C), as shown in Figure 3.

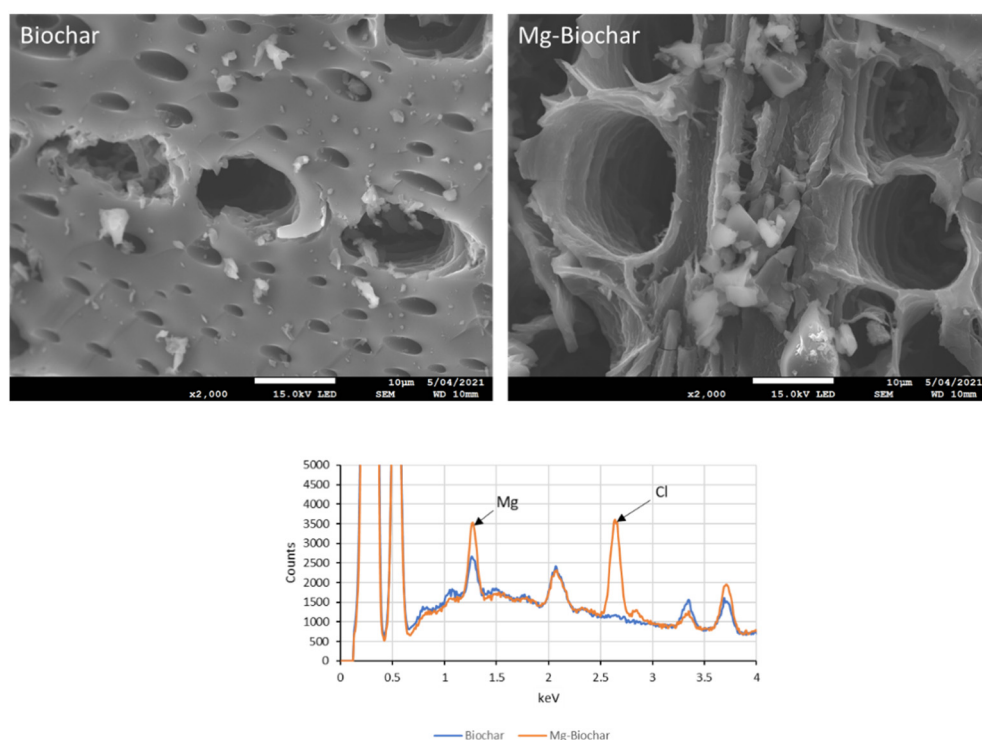


Figure 2. SEM scans and EDS spectrum of the biochar before and after modification.

FTIR analysis was performed to analyse the functional groups in both raw and modified biochar. The resulting FTIR spectra are shown in Figure 4. Biochar produced at 350 °C exhibited a broad band between 3000 and 3500 cm^{-1} (peak maximum at 3327 cm^{-1}) which represents vibrations of hydrogen-bonded O-H groups (alcoholic and phenolic) as well as the double-bonded groups C=O broad band between 1500 and 2000 cm^{-1} (peak maximum at 1689 cm^{-1}) [14]. For all raw biochar, adsorption in the region between 2843 and 2981 cm^{-1} C-H stretching is allocated to aliphatic functional groups and another strong band at 1055 cm^{-1} represents the C-O stretching oxygenated groups. The strong band at 1224 cm^{-1} represents phenolic -OH groups [42]. As temperature increases from 350 to 550 °C, OH functional groups, as well as C=O groups, decrease.

The strong aromatic band of C=C at 1602 cm^{-1} is observed in the biochar synthesised at 350 °C, and this vibration is strongly present until the temperature reached 550 °C, at which the band is reduced. This behaviour in biochar produced at high temperatures can be related to their low H/C ratio according to Zhang and Chen [48]. The intensities of C-H (2843 and 2981 cm^{-1}) aliphatic stretching, -OH phenolic (1224 cm^{-1}) and C-O bands (1055 cm^{-1}) exhibited a significant decrease because of the dehydration and degradation of ligneous and cellulosic compounds [43]. Functional groups present after modification of biochar by MgCl_2 and adsorption of phosphorus are shown in Figure 4. There is a significant peak for all biochar in the band stretching from 1500 to 2000 cm^{-1} (1578 cm^{-1}), indicating functional groups C=C and C=O aromatic bonds for modified biochar and modified biochar loaded with phosphorus as well as for raw biochar loaded with phosphorus. For modified biochar in the bands of 3299 and 699 cm^{-1} , groups assigned Mg-OH and

Mg-O were detected confirming the incorporation of Mg in the biochar [25,49]. Another significant change for biochar after modification was a sharp increase in the band 1577 cm^{-1} for all biochar samples except raw biochar, which can be attributed to the aromatic functional groups C=C and C=O. Compared with raw biochar, Mg-biochar contained groups in the intensity bands from 2500 to 3000 cm^{-1} (2906 cm^{-1}) and 1000 to 1500 cm^{-1} and these were assigned to CH_2 groups and C-O groups [50]. After the HW-biochar and Mg-biochar were loaded with phosphorus, a significant increase in the stretching bands of 1408 , 1023 , 874 and 559 cm^{-1} were observed for HW-biochar with functional groups C-H alkene, C-O and C-H aromatic out of plane. Regarding modified biochar, with the loading of P, the peaks located at 3299 and 699 cm^{-1} disappeared, indicating this group can be linked to the adsorption of phosphorus into the Mg-biochar [25].

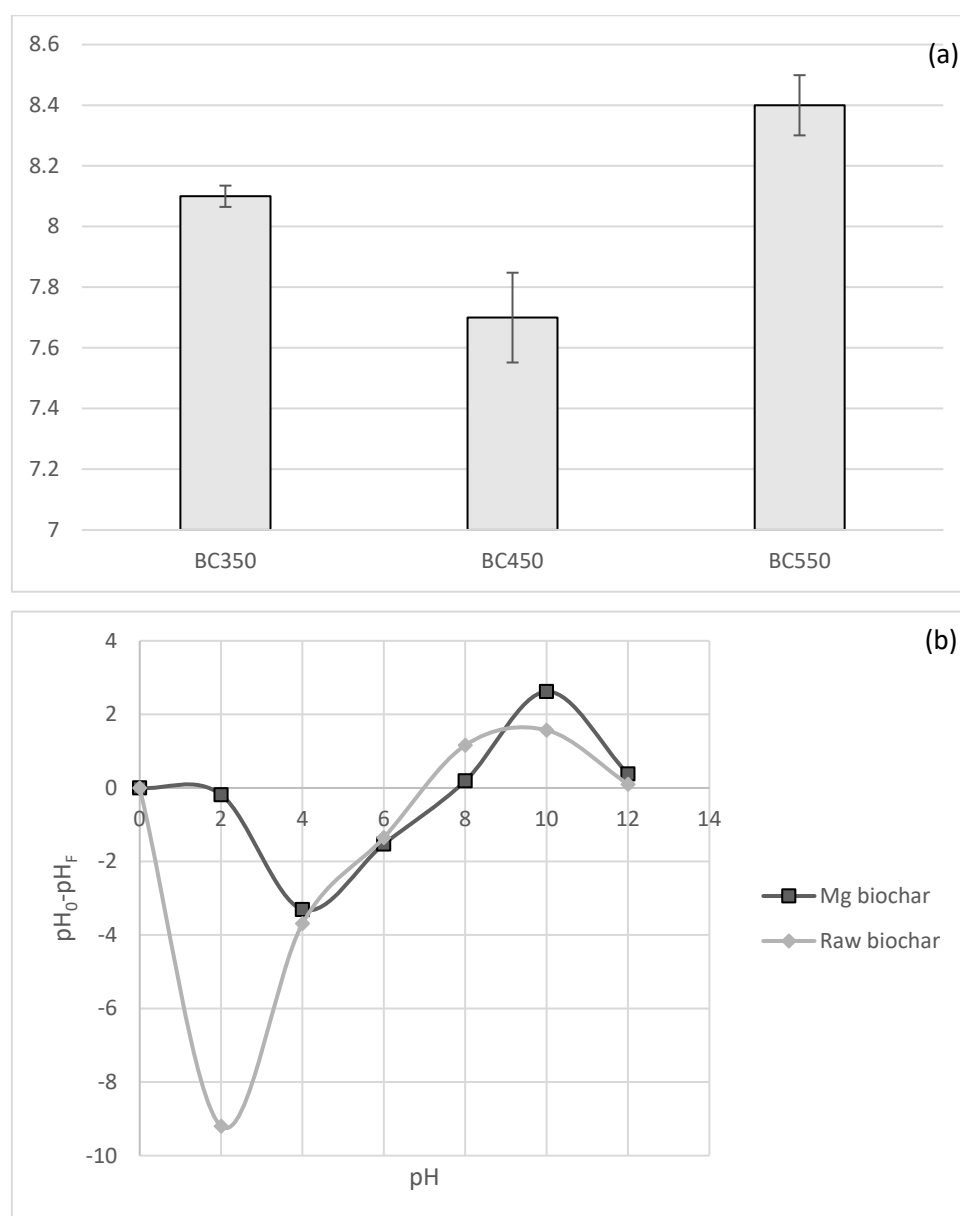


Figure 3. (a) pH values of raw biochar obtained from the pyrolysis of hardwood; and (b) point of zero charged pH_{PZC} from raw biochar and modified biochar (550 °C).

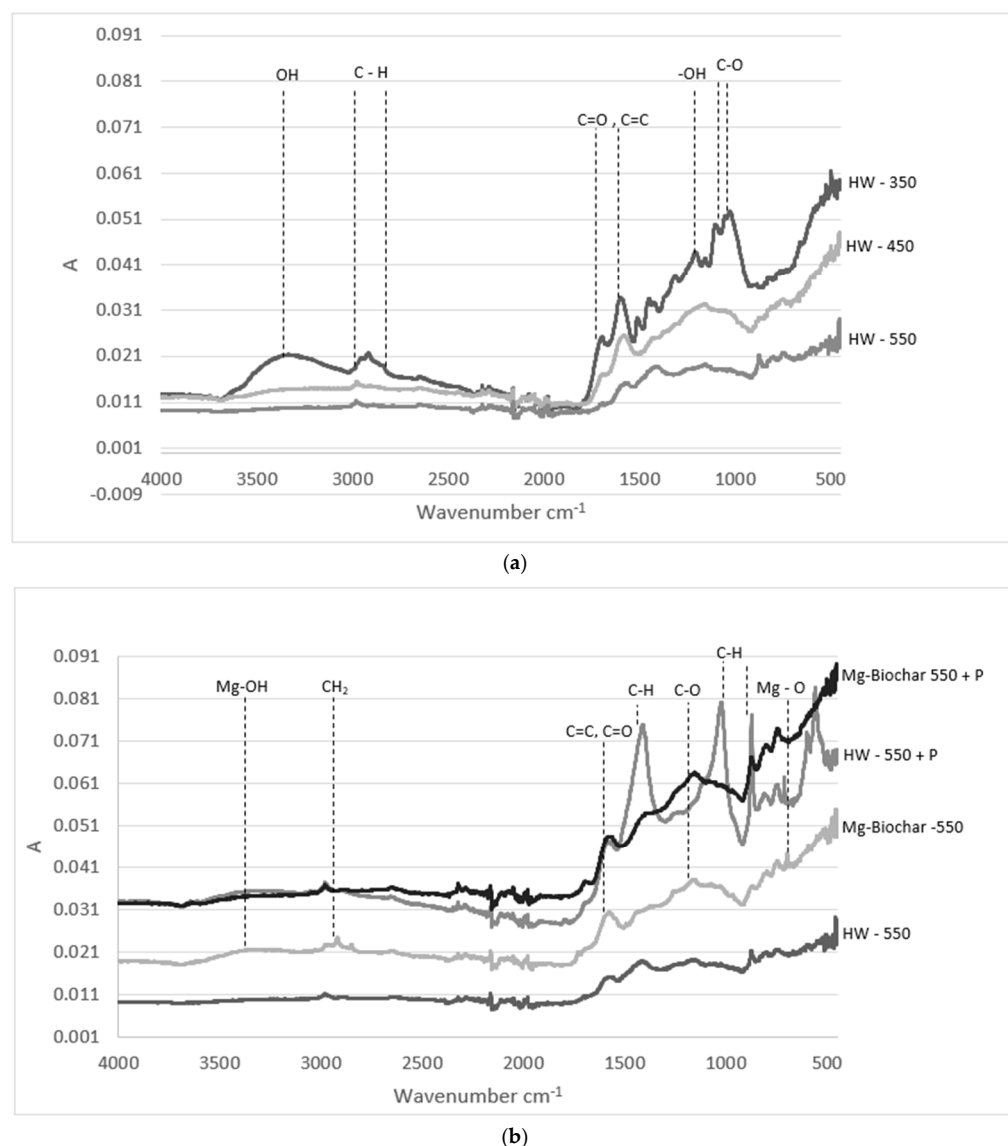


Figure 4. Fourier-transform infrared spectroscopy: (a) biochars prepared at different pyrolysis temperatures; and (b) modified and unmodified biochar before and after P adsorption.

3.2. Adsorption of Phosphorus by HW-Biochar and Mg-Biochar

The phosphorus adsorption capacities of raw biochar (HW-biochar) and Mg modified biochar (Mg-biochar) are shown in Figure 5. The raw biochar pyrolysed at 350 and 450 °C showed low adsorption capacity (0.26 and 0.25 mg-P·g⁻¹, respectively), as shown in Figure 5a. On the other hand, raw biochar synthesised at 550 °C showed the highest adsorption of phosphorus with 0.44 mg-P·g⁻¹; although the ANOVA test failed to confirm that the results were significantly different ($p = 0.22$), the BC550 adsorbed almost double the amount of phosphate compared to the other biochars. As pyrolysis temperature increases, biochar surface area and pore formation increase enhancing biochar adsorption capacity of phosphorus [26,51]. Similar results were found by Zhou and Xu [52] and Yin and Liu [25] with the increase in adsorption capacity of P for raw biochar with an increase in pyrolysis temperature. Because of its adsorption capacity, HW-biochar at 550 °C was chosen to be modified with Mg.

Biochar pyrolysed at 550 °C was selected to be modified with MgCl₂. Modified biochar with Mg showed an increase in the adsorption of P from 0.44 to 0.59 mg-P·g⁻¹ (Figure 5). Although t-test failed to confirm the significance of the improvement ($p = 0.2$), the change represents 34% improvement over unmodified biochar. Improvement in the performance of biochar by the addition of Mg has been presented in the literature. Fang

and Zhang [24] reported maximum adsorption of P of modified corn biochar was higher compared to raw biochar (239 and 225 mg·g⁻¹). Similar results were published by Yin and Liu [25], describing biochar modified with Mg dramatically increased phosphate adsorption. However, the results reported in [24,25] were obtained using extremely high initial concentrations of phosphate solutions. The Mg-biochar developed in this study was also able to achieve 238 mg·g⁻¹ when it was subjected to PO₄-P solution with initial concentration of 30 g·L⁻¹. The dramatic increase may be explained by the increased driving force due to the extreme difference between the PO₄-P concentration in the solid and liquid phases. The modification with magnesium proved to be crucial for enhancing the adsorption capacity of raw biochar as it increased the positive surface charge on the biochar, thus increasing the tendency to attract anions. Mg modified biochar in the literature has shown a high affinity to anions due to the high pH_{PZC} (12), as this causes the surface to be positively charged [45,53]. In our study, the HW-biochar and Mg-biochar pH_{PZC} values were 7.0 and 7.9. As the pH_{PZC} was higher than pH from the solution (pH = 5), a positive surface in the Mg-biochar can be expected, which, due to electrostatic adsorption between the adsorbate and the biochar, can contribute to improving adsorption of PO₄³⁻ [6,25]. Moreover, the adsorption of phosphate increased 34% over the raw biochar to Mg-biochar despite the decrease in the SSA.

Figure 6 shows the EDS spectra of the biochar before and after adsorption. It can be seen that Mg has played a role in phosphate adsorption in the unmodified and modified biochar. However, Mg's role can be easily seen in the modified biochar with the peak around 1.27 (corresponding to Mg) disappearing after adsorption. It can also be seen that the chloride (around 2.65) and calcium (3.73) have also have been involved in the adsorption of phosphate. Marshall and Morton [54] proposed a multi-step mechanism for the formation of calcium phosphate on biochar in which Cl⁻ played an important role. We propose a similar mechanism for the formation of magnesium phosphate on biochar.

3.3. Adsorption Isotherms

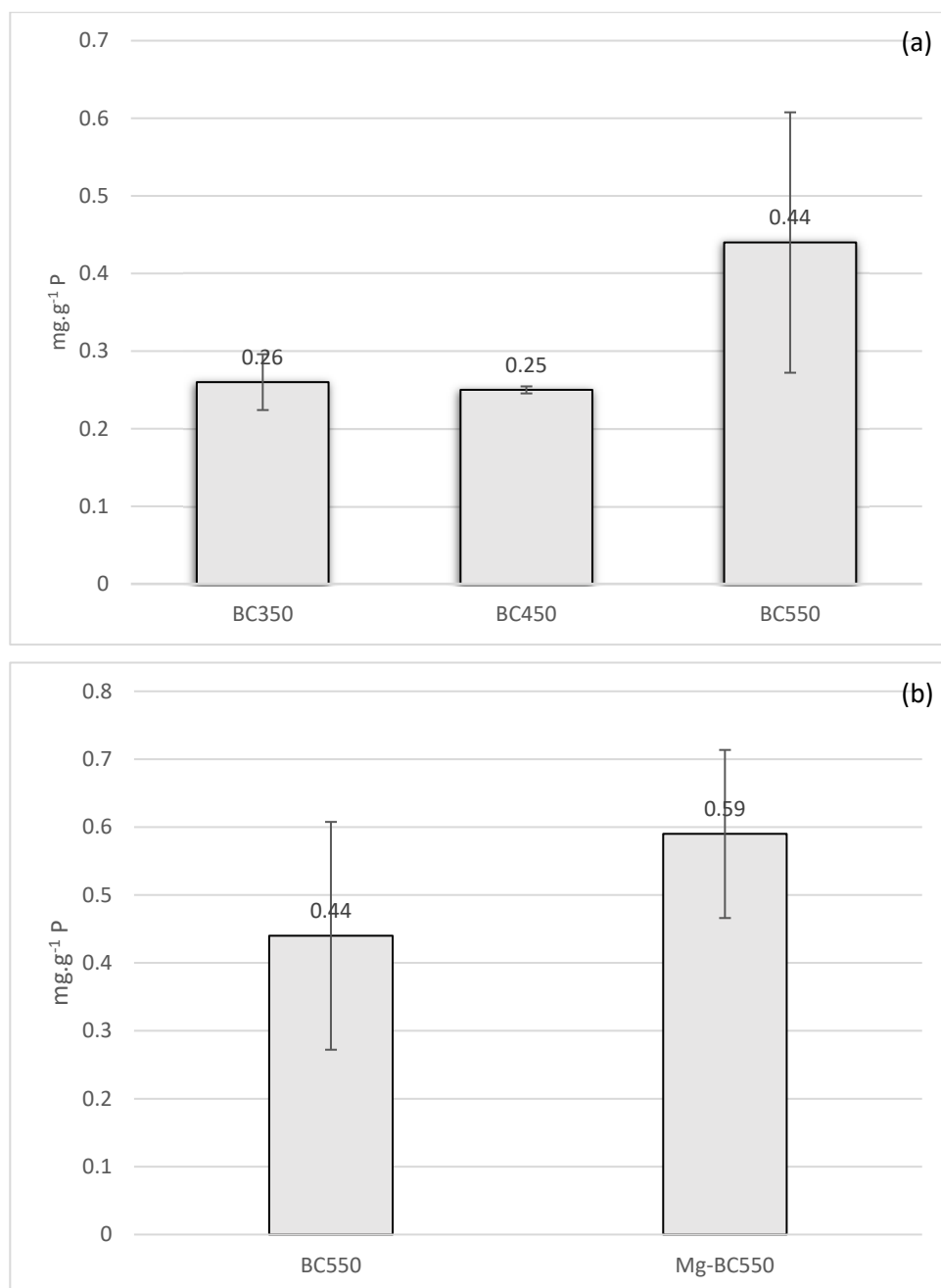
Figure 7 shows the adsorption isotherm for the Mg-modified biochar produced at 550 °C. The isotherm parameters for both models, including the determination coefficients (R²) and the root mean squared error (RMSE), are presented in Table 4. The Langmuir model describes homogenous adsorption in which all sites have equal affinity for the adsorbate [55]. On the other hand, the Freundlich model describes multilayer adsorption but with non-uniform distribution implied. The Langmuir maximum adsorption capacity of Mg-biochar was 463.5 mg PO₄-P·g⁻¹; however, this is unlikely to be achieved at realistic P concentrations. To confirm this, an adsorption experiment was conducted with initial PO₄-P concentration 30 g·L⁻¹ and found q_e to be 283 mg·g⁻¹. This behaviour may suggest that the adsorption is not conformant to Type I adsorption isotherm, which may violate the inherent assumption of Langmuir and Freundlich isotherm equations of Type I adsorption. Therefore, the results of the fitting from the models used in this study should be interpreted with caution. Table 5 shows selected values from reported P adsorption capacities of different Mg modified biochar. However, comparisons should proceed with caution as it is difficult to directly compare the values due to variations in experimental conditions. Furthermore, the reported q_{max} values are based on Langmuir calculated maximum capacity which may entail extrapolating the results beyond the experimental range.

Table 4. Langmuir and Freundlich isotherms parameters for the PO₄ adsorption using Mg-biochar.

Langmuir Model				Freundlich Model			
q _{max} (mg PO ₄ -P·g ⁻¹)	K _L (L·g ⁻¹)	R ²	RMSE	K _F	n	R ²	RMSE
463.5	3.65 × 10 ⁻⁵	0.78	0.17	6.05 × 10 ⁻⁶	0.31	0.89	0.12

Table 5. Adsorption capacities of PO₄ by other biochar modified with Mg.

Biochar Feedstock	Pyrolysis Temperature °C/Residence Time	C ₀ of Phosphate mg·L ⁻¹	q _{max} (mg PO ₄ -P·g ⁻¹)	References
Longleaf Pine	500/30 min	10 to 600	4.97	[45]
Red Oak	500/30 min	10 to 600	6.72	[45]
Poplar chips	600/2 h	100 to 500	28.94	[25]
Sugarcane crop	550/1 h	1 to 500	129.49	[53]
Hardwood	550/1.5 h	5 to 30	463.5	This study

**Figure 5.** Adsorption of P by: (a) unmodified biochar at different pyrolysis temperatures; and (b) unmodified and Mg modified biochar at 550 °C (mean ± standard deviation).

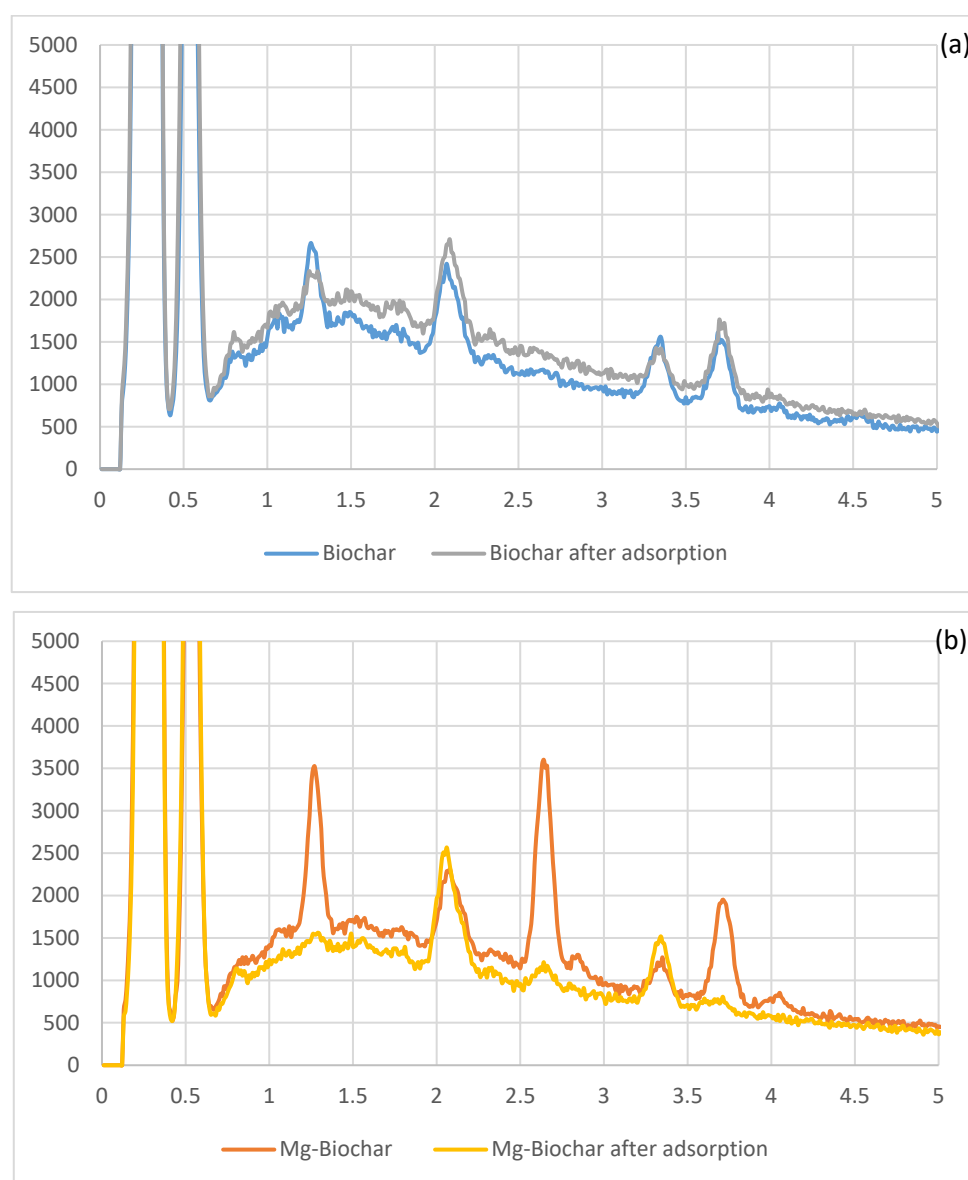


Figure 6. EDS scans before and after adsorption: (a) unmodified biochar; and (b) modified biochar.

3.4. Adsorption Kinetics

The adsorption of phosphate by Mg-biochar as a function of time is presented in Figure 8. It is clear that adsorption of PO_4^{3-} at the initial time is fast and then becomes relatively slow. Maximum adsorption was reached in 60 min. The fast initial adsorption of PO_4^{3-} can be caused by electrostatic forces between the positively charged Mg surface and the slow adsorption later might be due to intraparticle diffusion [5,53,56]. The data from the kinetic experiment were further fitted using the pseudo-first- (PFO) and pseudo-second-order (PSO) kinetic models. The pseudo-first- and the pseudo-second-order models fitted the experimental data with correlation coefficients $R^2 = 0.71$ and 0.73 , respectively. The fitted parameters are shown in Table 6. The PSO model assumes the mechanism of P adsorption onto Mg-biochar can be determined by chemisorption interaction, which agrees with the isotherm results [5,53].

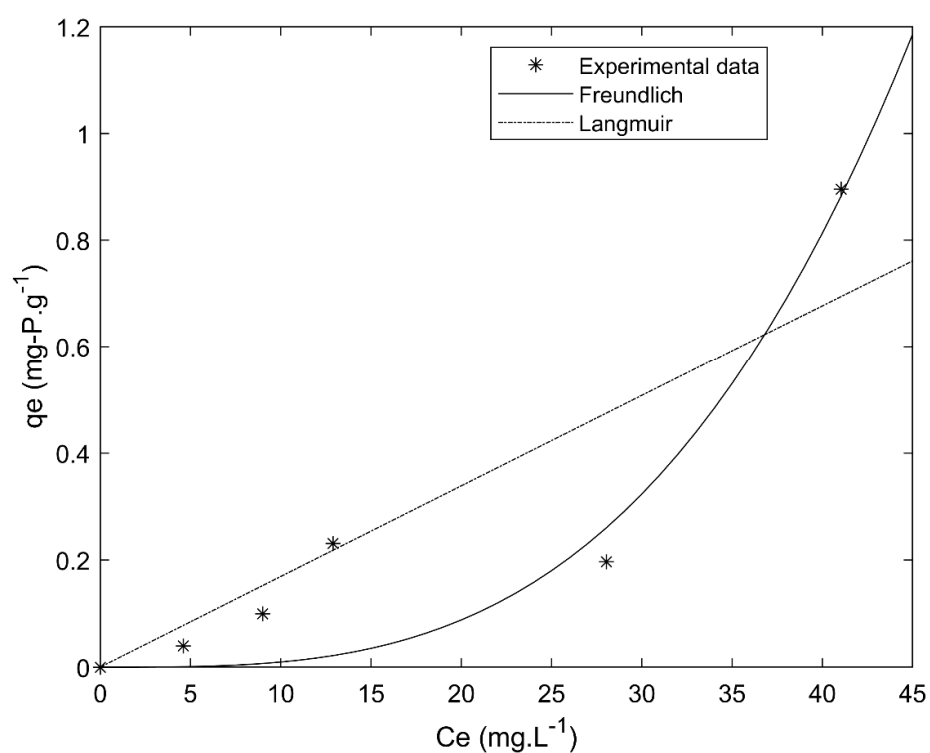


Figure 7. Phosphate adsorption isotherms of Mg-biochar derived from pyrolysis of hardwood.

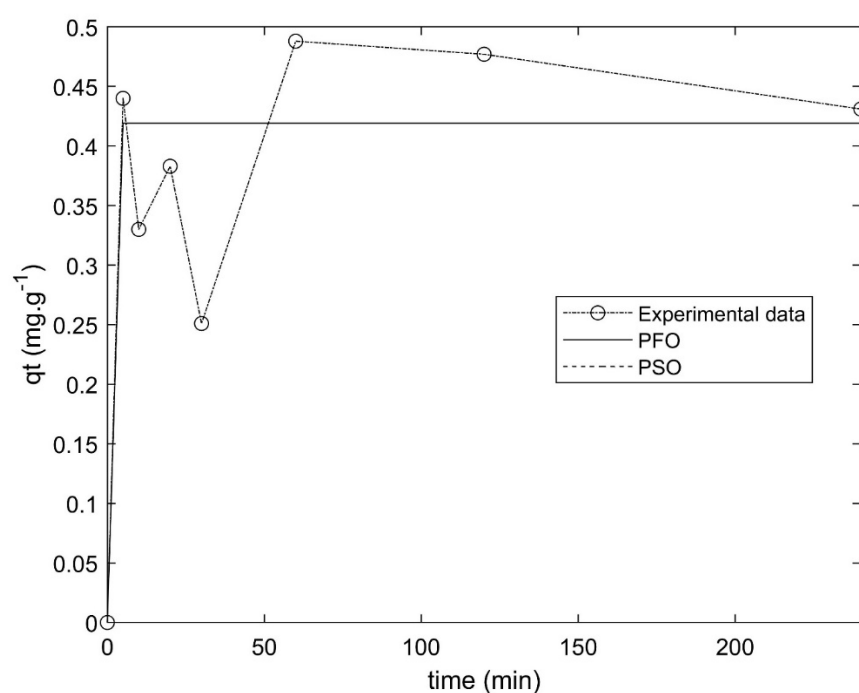


Figure 8. Adsorption kinetics data and modelling for P adsorption on the Mg-biochar.

Table 6. Kinetics models fitting parameters.

Parameter	PFO	PSO
k	4.75	1.819
qe	0.4192	0.4436
R ²	0.71	0.73
RMSE	0.095	0.092

The kinetics data indicate a degree of overshooting behaviour with q_t oscillating as time progresses. One possibility to explain this phenomenon is that, as the biochar has more active positive surface due to the addition of Mg, P is attached to this surface; however, the bonding seems to be weak. When the surface of biochar reaches the critical charge density, the new surface charge of biochar is negative because of the phosphate, therefore it starts repelling the incoming phosphate (Figure 9), which looks like there is a release instead of adsorption until equilibrium is reached.

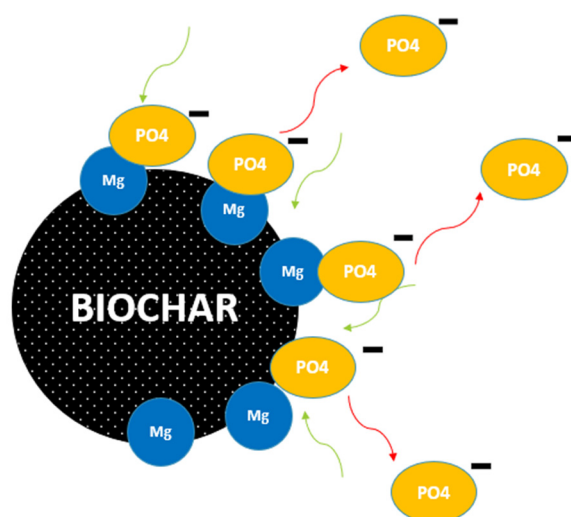


Figure 9. Overshooting phenomena of Mg-biochar.

3.5. Desorption of P from Mg-Biochar

The phosphate release was found to be higher in acidic than in neutral environments, as shown in Figure 10. This is expected, given the dissociation of magnesium and calcium phosphate behaviours. The initial loading of the biochar did not have significant impact on the rate or quantity of the phosphate released. In the case of acidic environment, within the first 5 min the phosphate concentration released reached $10.6 \text{ mg PO}_4\text{-P}\cdot\text{L}^{-1}$ and then remained relatively constant, most likely due to reaching equilibrium between the liquid–solid phase. This demonstrates that Mg-biochar can be used as a carrier to deliver phosphate, but it may not be suitable as a slow-release medium in acidic soils. On the other hand, in neutral environment, the rate of phosphate release was much slower ($\sim 5.5\%$) in 24 h with the curve showing the release continue to climb over time. This percentage is higher than the values reported by Fang and Zhang [24] for Mg biochar derived from corn with release values of 4.4% over a period of 90 h. This suggests that Mg-biochar may be a good carrier for slow delivery of phosphate in neutral soils.

Judging by the R^2 and RMSE values shown in Table 7, the release of the phosphate followed the bi-phasic desorption model with the fast release component being more prominent in the acidic environment mainly due to the solubilisation of magnesium phosphate. In the case of the neutral environment ($\text{pH} = 7$), only a small fraction of the adsorbed phosphate is immediately available, while the majority of the adsorbed phosphate is being held in the slow-release component. This can be very useful if the biochar is to be used as a carrier for the delivery of phosphate in agricultural applications as the fast release component can provide the phosphate during plant establishment while the slow-release component can ensure steady supply over extended periods of time.

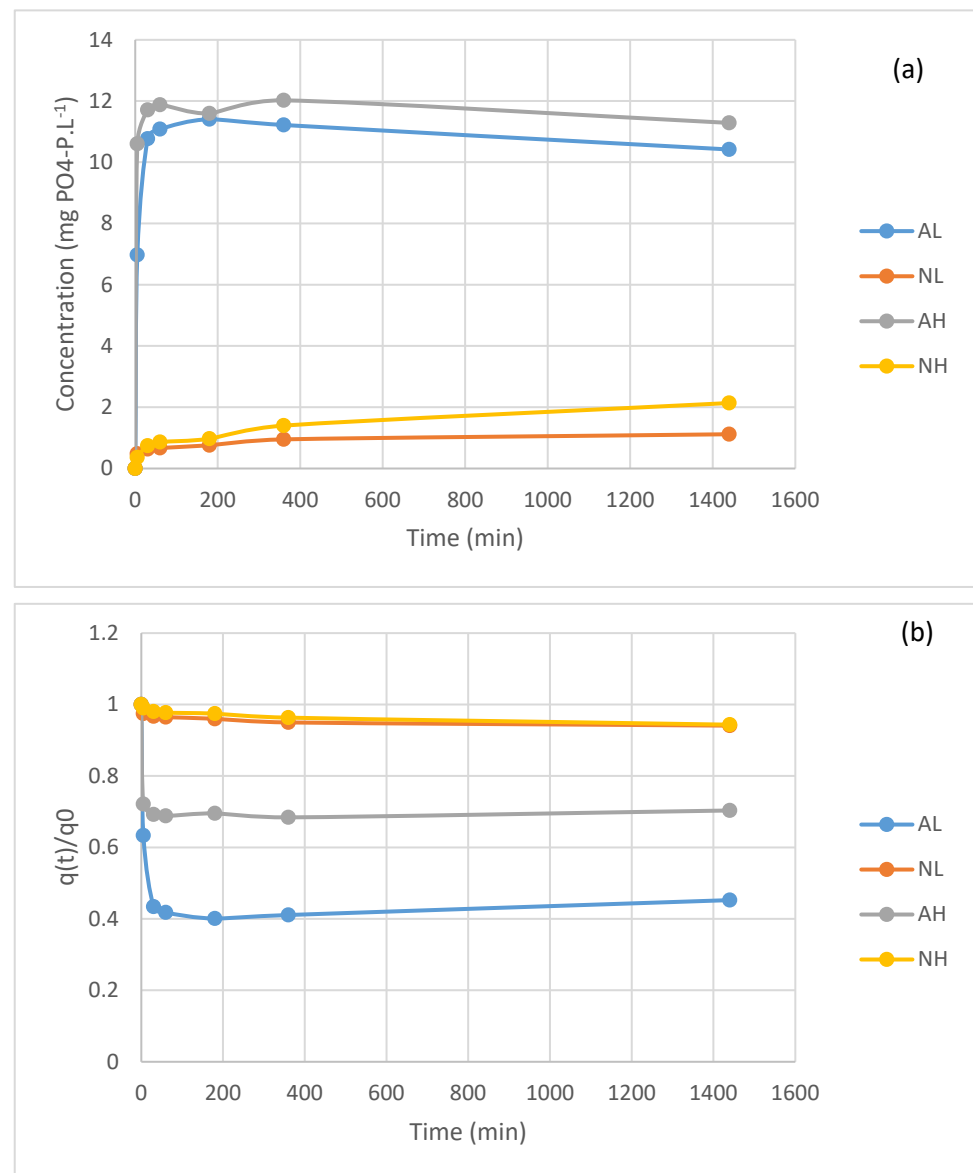


Figure 10. Phosphate release overtime (AL: pH = 4.6, initial loading = $1.904 \text{ mg} \cdot \text{g}^{-1}$; AH: pH = 4.6, initial loading = $3.875 \text{ mg} \cdot \text{g}^{-1}$; NL: pH = 7, initial loading = $1.904 \text{ mg} \cdot \text{g}^{-1}$ and NH: pH = 7, initial Loading = $3.875 \text{ mg} \cdot \text{g}^{-1}$).

Table 7. Desorption two term exponential model fitting parameters.

FRD					
Desorption Environment	q_0	k	R^2	RMSE	
AL	1.104	3.048×10^{-4}	0.09628	0.4358	
AH	2.884	7.731×10^{-5}	0.06052	0.4648	
NL	1.853	2.678×10^{-5}	0.494	0.3928	
NH	3.751	3.234×10^{-5}	0.7788	0.03592	
TFRC					
Desorption Environment	a	k_f	k_s	R^2	RMSE
AL	0.5754	-0.2017	-1.342×10^{-4}	0.9988	0.01293
AH	0.3072	-0.4727	-2.49×10^{-5}	0.9993	0.005097
NL	0.03642	-0.2318	-1.761×10^{-5}	0.9277	0.005075
NH	0.02195	-0.05333	-2.415×10^{-5}	0.9801	0.003657

4. Conclusions

Impregnation of biochar with Mg enhanced the phosphate adsorption capacity of the biochar by 34%. Formation of magnesium phosphate is the likely cause for the observed increase in capacity. The adsorption isotherm was best described by the Freundlich isotherm model and the kinetics were best described by the pseudo-second-order equation, suggesting that multiple mechanisms were involved in the adsorption of phosphate. Desorption experiments revealed that the desorption behaviour of the phosphate from biochar follows bi-phasic exponential decay model with fast- and slow-release components. The pH plays an important role in determining the distribution of the phosphate between the fast- and slow-release components. This behaviour is very useful if the exhausted biochar were to be used as a carrier for phosphate delivery in agricultural settings. The fast release component can provide the phosphate dose required during plant establishment while the slow-release component ensures the steady supply of phosphate over extended periods of time.

Author Contributions: Conceptualisation, A.E.H.; methodology, A.E.H.; software, L.A.B. and A.E.H.; validation, A.E.H.; formal analysis, L.A.B. and A.E.H.; investigation, L.A.B. and Z.M.; resources, A.E.H. and C.P.; data curation, L.A.B.; writing—original draft preparation, L.A.B.; writing—review and editing, A.E.H., Z.M. and C.P.; visualisation, L.A.B. and A.E.H.; supervision, A.E.H.; project administration, A.E.H. and C.P.; and funding acquisition, C.P. and A.E.H. All authors have read and agreed to the published version of the manuscript.

Funding: This research was funded by Griffith University’s School of Environment and Science ENGAGE Initiative.

Institutional Review Board Statement: No human or animal subjects were involved in this study. Note applicable.

Informed Consent Statement: Not applicable.

Data Availability Statement: Data are contained within the article.

Conflicts of Interest: The authors declare no conflict of interest.

References

1. Takaya, C.; Fletcher, L.; Singh, S.; Anyikude, K.; Ross, A. Phosphate and ammonium sorption capacity of biochar and hydrochar from different wastes. *Chemosphere* **2016**, *145*, 518–527. [[CrossRef](#)] [[PubMed](#)]
2. Qian, T.; Zhang, X.; Hu, J.; Jiang, H. Effects of environmental conditions on the release of phosphorus from biochar. *Chemosphere* **2013**, *93*, 2069–2075. [[CrossRef](#)]
3. Jung, K.-W.; Lee, S.; Lee, Y.J. Synthesis of novel magnesium ferrite (MgFe₂O₄)/biochar magnetic composites and its adsorption behavior for phosphate in aqueous solutions. *Bioresour. Technol.* **2017**, *245*, 751–759. [[CrossRef](#)]
4. Xu, K.; Zhang, C.; Dou, X.; Ma, W.; Wang, C. Optimizing the modification of wood waste biochar via metal oxides to remove and recover phosphate from human urine. *Environ. Geochem. Health* **2019**, *41*, 1767–1776. [[CrossRef](#)]
5. Wu, L.; Wei, C.; Zhang, S.; Wang, Y.; Kuzyakov, Y.; Ding, X. MgO-modified biochar increases phosphate retention and rice yields in saline-alkaline soil. *J. Clean. Prod.* **2019**, *235*, 901–909. [[CrossRef](#)]
6. Yin, Q.; Wang, R.; Zhao, Z. Application of Mg-Al-modified biochar for simultaneous removal of ammonium, nitrate, and phosphate from eutrophic water. *J. Clean. Prod.* **2018**, *176*, 230–240. [[CrossRef](#)]
7. Jung, K.-W.; Ahn, K.-H. Fabrication of porosity-enhanced MgO/biochar for removal of phosphate from aqueous solution: Application of a novel combined electrochemical modification method. *Bioresour. Technol.* **2016**, *200*, 1029–1032. [[CrossRef](#)]
8. Saxena, J.; Rawat, J.; Kumar, R. Conversion of biomass waste into biochar and the effect on Mung bean crop production. *Clean Soil Air Water* **2017**, *45*. [[CrossRef](#)]
9. Ding, Y.; Liu, Y.; Liu, S.; Huang, X.; Li, Z.; Tan, X.; Zeng, G.; Zhou, L. Potential benefits of biochar in agricultural soils: A review. *Pedosphere* **2017**, *27*, 645–661. [[CrossRef](#)]
10. Kavitha, B.; Reddy, P.V.L.; Kim, B.; Lee, S.S.; Pandey, S.K.; Kim, K.-H. Benefits and limitations of biochar amendment in agricultural soils: A review. *J. Environ. Manag.* **2018**, *227*, 146–154. [[CrossRef](#)] [[PubMed](#)]
11. Morales, M.M.; Comerford, N.; Guerrini, I.A.; Falcão, N.P.S.; Reeves, J.B. Sorption and desorption of phosphate on biochar and biochar-soil mixtures. *Soil Use Manag.* **2013**, *29*, 306–314. [[CrossRef](#)]
12. Amin, F.R.; Huang, Y.; He, Y.; Zhang, R.; Liu, G.; Chen, C. Biochar applications and modern techniques for characterization. *Clean Technol. Environ. Policy* **2016**, *18*, 1457–1473. [[CrossRef](#)]
13. Ndirangu, S.M.; Liu, Y.; Xu, K.; Song, S. Risk evaluation of pyrolyzed biochar from multiple wastes. *J. Chem.* **2019**, *2019*, 4506314. [[CrossRef](#)]

14. Tomczyk, A.; Sokołowska, Z.; Boguta, P. Biochar physicochemical properties: Pyrolysis temperature and feedstock kind effects. *Rev. Environ. Sci. Bio/Technol.* **2020**, *19*, 191–215. [\[CrossRef\]](#)
15. Dugdug, A.A.; Chang, S.X.; Ok, Y.S.; Rajapaksha, A.U.; Anyia, A. Phosphorus sorption capacity of biochars varies with biochar type and salinity level. *Environ. Sci. Pollut. Res.* **2018**, *25*, 25799–25812. [\[CrossRef\]](#)
16. Mukome, F.N.D.; Zhang, X.; Silva, L.C.R.; Six, J.; Parikh, S.J. Use of chemical and physical characteristics to investigate trends in biochar feedstocks. *J. Agric. Food Chem.* **2013**, *61*, 2196–2204. [\[CrossRef\]](#)
17. Man, Y.; Chen, Y. Enhanced phosphate adsorption on Ca-Mg-loaded biochar derived from tobacco stems. *Water Sci. Technol.* **2018**, *78*, 2427–2436.
18. Chen, Q.; Qin, J.; Sun, P.; Cheng, Z.; Shen, G. Cow dung-derived engineered biochar for reclaiming phosphate from aqueous solution and its validation as slow-release fertilizer in soil-crop system. *J. Clean. Prod.* **2018**, *172*, 2009–2018. [\[CrossRef\]](#)
19. Yang, Q.; Wang, X.; Luo, W.; Sun, J.; Xu, Q.; Chen, F.; Zhao, J.; Wang, S.; Yao, F.; Wang, D.; et al. Effectiveness and mechanisms of phosphate adsorption on iron-modified biochars derived from waste activated sludge. *Bioresour. Technol.* **2018**, *247*, 537–544. [\[CrossRef\]](#) [\[PubMed\]](#)
20. Wang, Z.; Guo, H.; Shen, F.; Yang, G.; Zhang, Y.; Zeng, Y.; Wang, L.; Xiao, H.; Deng, S. Biochar produced from oak sawdust by Lanthanum (La)-involved pyrolysis for adsorption of ammonium (NH_4^+), nitrate (NO_3^-), and phosphate (PO_4^{3-}). *Chemosphere* **2015**, *119*, 646–653. [\[CrossRef\]](#)
21. Micháleková-Richveisová, B.; Frišták, V.; Pipiška, M.; Ďuriška, L.; Moreno-Jimenez, E.; Soja, G. Iron-impregnated biochars as effective phosphate sorption materials. *Environ. Sci. Pollut. Res.* **2017**, *24*, 463–475. [\[CrossRef\]](#)
22. Wang, Z.; Shen, D.; Shen, F.; Li, T. Phosphate adsorption on lanthanum loaded biochar. *Chemosphere* **2016**, *150*, 1–7. [\[CrossRef\]](#)
23. Kuppusamy, S.; Thavamani, P.; Megharaj, M.; Venkateswarlu, K.; Naidu, R. Agronomic and remedial benefits and risks of applying biochar to soil: Current knowledge and future research directions. *Environ. Int.* **2016**, *87*, 1–12. [\[CrossRef\]](#)
24. Fang, C.; Zhang, T.; Li, P.; Jiang, R.-F.; Wang, Y.-C. Application of magnesium modified corn biochar for phosphorus removal and recovery from swine wastewater. *Int. J. Environ. Res. Public Health* **2014**, *11*, 9217–9237. [\[CrossRef\]](#)
25. Yin, Q.Q.; Liu, M.T.; Ren, H.P. Removal of ammonium and phosphate from water by Mg-modified biochar: Influence of Mg pretreatment and pyrolysis temperature. *Bioresources* **2019**, *14*, 6203–6218.
26. Takaya, C.; Fletcher, L.; Singh, S.; Okwuosa, U.; Ross, A. Recovery of phosphate with chemically modified biochars. *J. Environ. Chem. Eng.* **2016**, *4*, 1156–1165. [\[CrossRef\]](#)
27. Wan, S.; Wang, S.; Li, Y.; Gao, B. Functionalizing biochar with Mg-Al and Mg-Fe layered double hydroxides for removal of phosphate from aqueous solutions. *J. Ind. Eng. Chem.* **2017**, *47*, 246–253. [\[CrossRef\]](#)
28. Park, J.H.; Ok, Y.S.; Kim, S.H.; Cho, J.S.; Heo, J.S.; Delaune, R.D.; Seo, D.C. Evaluation of phosphorus adsorption capacity of sesame straw biochar on aqueous solution: Influence of activation methods and pyrolysis temperatures. *Environ. Geochem. Health* **2015**, *37*, 969–983. [\[CrossRef\]](#)
29. Liao, T.; Li, T.; Su, X.; Yu, X.; Song, H.; Zhu, Y.; Zhang, Y. La(OH)₃-modified magnetic pineapple biochar as novel adsorbents for efficient phosphate removal. *Bioresour. Technol.* **2018**, *263*, 207–213. [\[CrossRef\]](#) [\[PubMed\]](#)
30. Li, J.; Li, B.; Huang, H.; Zhao, N.; Zhang, M.; Cao, L. Investigation into lanthanum-coated biochar obtained from urban dewatered sewage sludge for enhanced phosphate adsorption. *Sci. Total. Environ.* **2020**, *714*, 136839. [\[CrossRef\]](#) [\[PubMed\]](#)
31. Wang, L.; Wang, J.; He, C.; Lyu, W.; Zhang, W.; Yan, W.; Yang, L. Development of rare earth element doped magnetic biochars with enhanced phosphate adsorption performance. *Colloids Surf. A Physicochem. Eng. Asp.* **2019**, *561*, 236–243. [\[CrossRef\]](#)
32. Yang, B.; Feng, Y.; Yu, Y.; He, S.; Liu, H.; Xue, L.; Yang, L. Lanthanum ferrite nanoparticles modification onto biochar: Derivation from four different methods and high performance for phosphate adsorption. *Environ. Sci. Pollut. Res.* **2019**, *26*, 22010–22020. [\[CrossRef\]](#) [\[PubMed\]](#)
33. Nguyen, T.A.; Ngo, H.H.; Guo, W.S.; Zhang, J.; Liang, S.; Tung, K.L. Feasibility of iron loaded ‘okara’ for biosorption of phosphorous in aqueous solutions. *Bioresour. Technol.* **2013**, *150*, 42–49. [\[CrossRef\]](#)
34. Li, Z.; Liu, X.; Wang, Y. Modification of sludge-based biochar and its application to phosphorus adsorption from aqueous solution. *J. Mater. Cycles Waste Manag.* **2019**, *22*, 123–132. [\[CrossRef\]](#)
35. Ren, J.; Li, N.; Li, L.; An, J.-K.; Zhao, L.; Ren, N.-Q. Granulation and ferric oxides loading enable biochar derived from cotton stalk to remove phosphate from water. *Bioresour. Technol.* **2015**, *178*, 119–125. [\[CrossRef\]](#) [\[PubMed\]](#)
36. Novais, S.V.; Zenero, M.D.O.; Barreto, M.S.C.; Montes, C.R.; Cerri, C.E.P. Phosphorus removal from eutrophic water using modified biochar. *Sci. Total. Environ.* **2018**, *633*, 825–835. [\[CrossRef\]](#) [\[PubMed\]](#)
37. Akgül, G.; Maden, T.B.; Diaz, E.; Jiménez, E.M. Modification of tea biochar with Mg, Fe, Mn and Al salts for efficient sorption of PO_4^{3-} and Cd^{2+} from aqueous solutions. *J. Water Reuse Desalination* **2019**, *9*, 57–66. [\[CrossRef\]](#)
38. Hale, S.E.; Alling, V.; Martinsen, V.; Mulder, J.; Breedveld, G.D.; Cornelissen, G. The sorption and desorption of phosphate-P, ammonium-N and nitrate-N in cacao shell and corn cob biochars. *Chemosphere* **2013**, *91*, 1612–1619. [\[CrossRef\]](#)
39. Mahdi, Z.; El Hanandeh, A.; Yu, Q. Influence of pyrolysis conditions on surface characteristics and methylene blue adsorption of biochar derived from date seed biomass. *Waste Biomass Valorization* **2016**, *8*, 2061–2073. [\[CrossRef\]](#)
40. Birdwell, J.; Cook, R.L.; Thibodeaux, L.J. Desorption kinetics of hydrophobic organic chemicals from sediment to water: A review of data and models. *Environ. Toxicol. Chem.* **2007**, *26*, 424–434. [\[CrossRef\]](#)
41. Chen, X.; Chen, G.; Chen, L.; Chen, Y.; Lehmann, J.; McBride, M.B.; Hay, A.G. Adsorption of copper and zinc by biochars produced from pyrolysis of hardwood and corn straw in aqueous solution. *Bioresour. Technol.* **2011**, *102*, 8877–8884. [\[CrossRef\]](#)

42. Domingues, R.R.; Trugilho, P.F.; Silva, C.A.; De Melo, I.C.N.A.; Melo, L.C.A.; Magriotis, Z.M.; Sánchez-Monedero, M.A. Properties of biochar derived from wood and high-nutrient biomasses with the aim of agronomic and environmental benefits. *PLoS ONE* **2017**, *12*, e0176884. [[CrossRef](#)]
43. Ola, F.; Jekayinfa, S. Pyrolysis of sandbox (*Hura crepitans*) shell: Effect of pyrolysis parameters on biochar yield. *Res. Agric. Eng.* **2016**, *61*, 170–176. [[CrossRef](#)]
44. Tag, A.T.; Duman, G.; Ucar, S.; Yanik, J. Effects of feedstock type and pyrolysis temperature on potential applications of biochar. *J. Anal. Appl. Pyrolysis* **2016**, *120*, 200–206. [[CrossRef](#)]
45. Oginni, O.; Yakaboylu, G.A.; Singh, K.; Sabolsky, E.M.; Unal-Tosun, G.; Jaisi, D.; Khanal, S.; Shah, A. Phosphorus adsorption behaviors of MgO modified biochars derived from waste woody biomass resources. *J. Environ. Chem. Eng.* **2020**, *8*. [[CrossRef](#)]
46. Lu, S.; Zong, Y. Pore structure and environmental serves of biochars derived from different feedstocks and pyrolysis conditions. *Environ. Sci. Pollut. Res.* **2018**, *25*, 30401–30409. [[CrossRef](#)] [[PubMed](#)]
47. Li, H.; Dong, X.; da Silva, E.B.; de Oliveira, L.M.; Chen, Y.; Ma, L.Q. Mechanisms of metal sorption by biochars: Biochar characteristics and modifications. *Chemosphere* **2017**, *178*, 466–478. [[CrossRef](#)] [[PubMed](#)]
48. Zhang, H.; Chen, C.; Gray, E.M.; Boyd, S.E. Effect of feedstock and pyrolysis temperature on properties of biochar governing end use efficacy. *Biomass Bioenergy* **2017**, *105*, 136–146. [[CrossRef](#)]
49. Cui, X.; Dai, X.; Khan, K.Y.; Li, T.; Yang, X.; He, Z. Removal of phosphate from aqueous solution using magnesium-alginate/chitosan modified biochar microspheres derived from *Thalia dealbata*. *Bioresour. Technol.* **2016**, *218*, 1123–1132. [[CrossRef](#)]
50. Coates, J. Interpretation of infrared spectra, A practical approach. In *Encyclopedia of Analytical Chemistry: Applications, Theory and Instrumentation*; John Wiley & Sons Ltd.: Chichester, UK, 2000; pp. 10815–10837.
51. Jung, K.-W.; Kim, K.; Jeong, T.-U.; Ahn, K.-H. Influence of pyrolysis temperature on characteristics and phosphate adsorption capability of biochar derived from waste-marine macroalgae (*Undaria pinnatifida* roots). *Bioresour. Technol.* **2016**, *200*, 1024–1028. [[CrossRef](#)] [[PubMed](#)]
52. Zhou, L.; Xu, D.; Li, Y.; Pan, Q.; Wang, J.; Xue, L.; Howard, A. Phosphorus and nitrogen adsorption capacities of biochars derived from feedstocks at different pyrolysis temperatures. *Water* **2019**, *11*, 1559. [[CrossRef](#)]
53. Li, R.; Wang, J.J.; Zhou, B.; Zhang, Z.; Liu, S.; Lei, S.; Xiao, R. Simultaneous capture removal of phosphate, ammonium and organic substances by MgO impregnated biochar and its potential use in swine wastewater treatment. *J. Clean. Prod.* **2017**, *147*, 96–107. [[CrossRef](#)]
54. Marshall, J.A.; Morton, B.J.; Muhlack, R.; Chittleborough, D.; Kwong, C.W. Recovery of phosphate from calcium-containing aqueous solution resulting from biochar-induced calcium phosphate precipitation. *J. Clean. Prod.* **2017**, *165*, 27–35. [[CrossRef](#)]
55. Foo, K.; Hameed, B. Insights into the modeling of adsorption isotherm systems. *Chem. Eng. J.* **2010**, *156*, 2–10. [[CrossRef](#)]
56. Huang, H.; Zhang, P.; Zhang, Z.; Liu, J.; Xiao, J.; Gao, F. Simultaneous removal of ammonia nitrogen and recovery of phosphate from swine wastewater by struvite electrochemical precipitation and recycling technology. *J. Clean. Prod.* **2016**, *127*, 302–310. [[CrossRef](#)]